

A possible gravitational lens in the Hubble Deep Field South

Rennan Barkana¹, Roger Blandford⁴, David W. Hogg²
Institute for Advanced Study, Olden Lane, Princeton, NJ 08540, USA

ABSTRACT

We model an apparent gravitational lens system HDFS 2232509–603243 in the Hubble Deep Field South. The system consists of a blue $V = 25$ mag arc separated by $0''.9$ from a red $V = 22$ mag elliptical galaxy. A mass distribution which follows the observed light distribution with a constant mass-to-light ratio can fit the arc component positions if external shear is added. A good fit is also obtained with simple parameterized models, and all the models predict a fourth image fainter than the detection limit. The inferred mass-to-light ratio is ~ 15 in solar units if the lens is at $z = 0.6$. The lens models predict a velocity dispersion of ~ 280 km s⁻¹ which could be confirmed with spectroscopy.

Subject headings: cosmology: observations — galaxies: individual (HDFS 2232509–603243) — gravitational lensing

1. Introduction

Detailed studies of gravitational lenses have provided a wealth of information on galaxies, both through modeling of individual lens systems (e.g., Schneider, Ehlers, & Falco 1992; Blandford & Narayan 1992) and from the statistical properties of multiply imaged sources (e.g., Turner, Ostriker, & Gott 1984; Kochanek 1996). The extraordinary resolution of the Hubble Space Telescope (HST) has allowed for the first time the detection of lenses where both the source and the deflector are “normal” optically-selected galaxies. Ratnatunga et al. (1995) discovered two four-image “Einstein cross” gravitational lenses in the Groth-Westphal strip. Their mass models required ellipticities substantially above those of the light distributions, suggesting (as is commonly suspected in radio lenses) that some external shear is important to the lensing.

The Hubble Deep Field (HDF, Williams et al. 1996), the deepest set of exposures taken with the HST, has enabled an unprecedented study of galaxy morphological evolution (e.g., Ellis 1998) and

¹email: barkana@ias.edu

²Hubble Fellow

⁴also California Institute of Technology, Pasadena, CA 91125

the global star formation history (e.g., Madau, Pozzetti, & Dickinson 1998). Candidate gravitational lenses were reported by Hogg et al. (1996), who noted on the basis of radio surveys that several lenses are expected in the HDF (cf. Cooray, Quashnock, & Miller 1998). However, after further observations not one strong case for multiple imaging has been identified (Zepf, Moustakas, & Davis 1997; Cohen 1998).

The Southern Hubble Deep Field (HDF-S, Williams et al. 1998) is a second set of ultra-deep HST exposures, and several lenses are again expected. The best candidate lens, noted by the HDF-S team (Williams 1998), consists of a blue arc about $0''.9$ from an elliptical galaxy. In this *Letter* we report on a detailed study of this arc and argue that it is a bona fide multiply imaged source.

2. Observations

The WFPC2 HDF-S is a ~ 5 arcmin² field centered on 22 32 56.22 – 60 33 02.69 (J2000), imaged with the WFPC2 instrument on the HST in the $F300W$, $F450W$, $F606W$, and $F814W$ bandpasses for total exposure times of 1.4×10^5 , 1.0×10^5 , 8×10^4 , and 1.0×10^5 s respectively, reaching point-source sensitivities of roughly $V = 29$ mag (Williams et al. 1998). For the “version-1.0” reductions of the images, we adopt the Vega-relative calibrations supplied by the HDF-S team whereby 1 DN corresponds to $F300W = 19.43$ mag, $F450W = 22.02$ mag, $F606W = 22.90$ mag, or $F814W = 21.66$ mag. The images clearly show a bright candidate lens system at pixel location (2982.7, 2837.6). With the pixel scale of $0''.0398$ this is also 22 32 50.90 – 60 32 43.0 (J2000). This candidate lens system will be called “HDFS 2232509–603243” hereafter.

The morphology of HDFS 2232509–603243 is that of a $V \sim 22$ mag elliptical galaxy (hereafter “the elliptical”) with a much bluer arc (hereafter “the arc”) located $0''.9$ to the NW from the center of the elliptical, as shown in Figure 1. There is also a faint point-like source (hereafter “the dot”) located $0''.96$ to the NE from the center of the elliptical.

The elliptical is smooth and symmetrical, so images created by rotating its images through 180° (centered on the pixel nearest the center of the elliptical) and subtracting them from their unrotated originals show essentially no sign of the elliptical. Photometry of the arc was performed in these “rotated-subtracted” images. The total $F606W$ flux (given in Table 1) was measured through a partial annulus of inner radius $0''.517$ and outer radius $1''.194$, extending over position angles 0° (north through east) through -108° . Colors were measured through a partial annulus of inner and outer radii $0''.677$ and $1''.035$, over -18° through -90° . The flux and colors of the dot were measured through a $0''.159$ radius circular aperture. Because nearby pixels are correlated, signal-to-noise ratios for photometric measurements were found by re-binning the image into pixels 4×4 times larger.

The arc separates into four distinct components, labeled A , B , C and D , going clockwise around the arc. All have very similar colors. Components A , B , and D appear to have point-like centers with fuzz, while component C is more extended. Gaussians with the same FWHM as the

PSF (4 pixels) were fit to components A , B and D , and a gaussian of variable width was fit to component C , all in the $F450W$ rotated-subtracted image. The best-fit positions and fluxes of these gaussians are given in Table 2.

In order to make arc-free images of the elliptical, the region of each image in the partial annulus centered on the elliptical with inner and outer radii of $0''.517$ and $1''.194$ and position angles 0° through -108° was replaced with the corresponding region diametrically opposite (i.e., at a position angle rotated by 180°). These “arc-removed” images show virtually no evidence of the arc. The total $F814W$ flux of the elliptical was measured out to its $2\text{-}\sigma$ (per pixel) isophote. The colors were measured through $0''.915$ radius circular apertures, and are given in Table 1.

A de Vaucouleurs profile is a very good fit to the azimuthally averaged radial profile of the elliptical in the “arc-removed” images. The effective radius is $r_e = 0''.31$ and the $F814W$ -band surface brightness at the effective radius is 21.0 mag in each arcsec². The isophote ellipticity orientation varies with radius. The outer isophotes (radii $> 0''.8$) of the elliptical have ellipticity ~ 0.2 and are elongated along $+40^\circ$. The inner isophotes (radii $< 0''.3$) also have ellipticity ~ 0.2 but are elongated along -40° , i.e., almost orthogonal. Isophotes intermediate to these two regimes are fairly circular.

Comparison of the colors of the elliptical with HDF galaxies with known redshifts suggests that its redshift is roughly $z = 0.6$ (cf. the photometric redshift of 0.5 of Gwyn (1998)). This suggests a total luminosity⁴ of $8.7 \times 10^9 h^{-2} L_\odot$ in the rest-frame B-band, or roughly L_* . The luminosity is a factor of 3 larger if $z = 0.8$, and a factor of 6.5 smaller if $z = 0.3$.

3. Lens models

We consider several models for the lensing mass distribution, simple parameterized models as well as a constant mass-to-light ratio model. The image positions are not very sensitive to the radial profile of the lens, so for the parameterized models we take it to be singular and isothermal. Asymmetry is required and we consider two types, external shear or an elliptical galaxy. We assume that the arc components A , B and D are three images of a common source, with A and B a merging pair. Component C can easily be produced if the source is extended or multi-component. We do not include as constraints component C or the observed flux ratios among components A , B and D , since these are sensitive to the detailed flux distribution of the source. We discuss the dot below.

We consider a lens at redshift z_L and a source at z_S . Then the lens mass distribution determines a convergence κ and a potential ψ (e.g., Schneider et al. 1992; Blandford & Narayan 1992). The singular isothermal sphere (SIS) is defined by $\kappa = b/[2r]$. We add to the potential the term $\psi_\gamma = -\frac{1}{2}\gamma r^2 \cos 2(\theta - \theta_\gamma)$, which defines an external shear of magnitude γ and direction θ_γ . If the

⁴We assume a world model of $\Omega = 0.3$ in matter and no cosmological constant, and also set $H_0 = 100 h \text{ km s}^{-1} \text{ Mpc}^{-1}$.

shear is due to an axisymmetric galaxy then it is located at an angle θ_γ from the lens galaxy. We denote by SIS+ γ the SIS model with external shear.

A singular isothermal elliptical mass distribution (SIEMD) with an axis ratio a and a major axis along the y -axis is given by $\kappa = b/[2\sqrt{x^2 + y^2a^2}]$. More generally we rotate the major axis by an angle θ_ϵ . The lensing properties of the SIEMD have been studied by Kassiola & Kovner (1993) and by Kormann, Schneider, & Bartelmann (1994).

We fit these two lens models, the SIS+ γ model and the SIEMD, to the three observed image positions, with results shown in Table 3. Both lens models have an elongated diamond caustic with four cusps. We indicate a source near a cusp on the major axis by [maj] and one near a minor cusp by [min]. Since the observed position B is farther from the center of the lens than A or D , the arc is more naturally produced by a minor cusp for which only the middle image of the three is outside the critical curve.

Interestingly, the orientation of the SIEMD[min] model agrees with the observed orientation of the elliptical’s outer isophotes, while the orientation of the SIEMD[maj] model agrees with that of the inner isophotes. However, among the simple parameterized models only the SIS+ γ [min] model fits the data well (see Table 3 and Figure 2). This model requires a substantial shear ($\gamma = 0.26$) produced by objects lying in the NE or SW directions. To compute the mass-to-light ratio for various models, we fix a circle about the galaxy center of radius $0''.915$. The luminosity of the galaxy within this circle is $7.6 \times 10^9 h^{-2} L_\odot$ if $z_L = 0.6$. If, e.g., $z_S = 1.5$, then the mass within the same circle of the SIS is $M = 2.1 \times 10^{11} h^{-1} (b/1'') M_\odot$. This yields a mass-to-light ratio of $27 h (b/1'')$, and a velocity dispersion $\sigma = 270 \sqrt{b/1''} \text{ km s}^{-1}$.

As a second approach to modeling, we utilize the resolved image of the lens galaxy (smoothed with a 4-pixel FWHM gaussian) to construct a model with a constant mass-to-light ratio (denoted M/L). The pure M/L model fails but together with external shear it produces an excellent fit, albeit with a large shear. Even a small shear such as 0.05 produces a substantially better fit than with no shear (see Table 3 and Figure 3). All the M/L models produce a minor cusp configuration. The parameter $\bar{\kappa}$ for the M/L models gives the mean κ in a circle of radius $0''.915$ about the galaxy center. If $z_L = 0.6$ and $z_S = 1.5$ then the mass within this circle is $M = 1.9 \times 10^{11} h^{-1} \bar{\kappa} M_\odot$, which yields a mass-to-light ratio of $25 h \bar{\kappa}$. If we assume a small shear then $\bar{\kappa} \sim 1$ (Table 3), and the mass-to-light ratio is on the high side of the range of other lens galaxies (Keeton, Kochanek, & Falco 1998). Note, however, that we only have an estimated photometric redshift for the lens and a guess for the source redshift. The mass-to-light ratio changes to $14 h \bar{\kappa}$ for ($z_L = 0.8, z_S = 2.0$) and to $57 h \bar{\kappa}$ for ($z_L = 0.3, z_S = 1.0$).

No fourth image is detected down to the detection threshold of about 28.9 mag in $F606W$. This is consistent with the models, which predict a fourth image fainter than the third by a factor of 3 or 4. The M/L models are non-singular and predict a fifth image fainter by an additional factor of ~ 100 . The best-fitting models also locate the image of the cusp near the observed position of component C , so this component can be produced if the source is extended.

Thus far we have not included the dot, assuming it to be a separate background source. We consider also the possibility that the dot is the third image corresponding to components A and B . The types of lens models used above can fit these alternative image positions with similar χ^2 values as in Table 3, but they fail since they predict an observable arc which includes counter images of components C and D and extends South-East from the dot. More elaborate lens models could work but only if the sources of components C and D are small (subpixel) and lie right on the caustic.

4. Discussion

We have modeled a candidate gravitational lens, HDF-S 2232509–603243, found in the HDF-S. The image positions can be fit in a minor cusp configuration by simple lens models which include ellipticity or shear, or with shear added to a model with a constant mass-to-light ratio. However, an exact fit is obtained only with a substantial shear produced by objects lying to the NE or SW. No obvious candidate galaxy lies within $5''$ of the lens, but there are several galaxies $\sim 20''$ to the SW and others $\sim 35''$ to the NE with photometric redshifts in the range 0.5–0.7 (Gwyn 1998). Spectroscopic redshifts will determine the possible presence of galaxy groups.

The lensing galaxy is expected to have a redshift $z \sim 0.6$, which gives it a luminosity of $\sim L^*$. Lens models imply a mass-to-light ratio of $\sim 25 h$, and a velocity dispersion of $\sim 280 \text{ km s}^{-1}$. If the elliptical falls on the fundamental plane, a central line-of-sight velocity dispersion of only $\sim 100 \text{ km s}^{-1}$ is expected if $z = 0.6$ (Jorgensen, Franx & Kjaergaard 1996), which suggests that $z \sim 0.8$ is more likely.

Showing that the arc and the lens galaxy are at different redshifts would rule out the possibility that the arc is a tidally disrupted satellite. On 10-m-class telescopes, it is straightforward to get spectroscopic redshifts of galaxies at 22 mag, even elliptical galaxies which tend to have absorption-feature dominated spectra (Cohen et al. 1998). Some elliptical galaxies at this flux level even have measured central velocity dispersions (van Dokkum et al. 1998; Pahre 1998). Thus the prospects for follow-up spectroscopy on the elliptical are good. It is common to obtain redshifts for sources at 25 mag, even some which are close to bright nearby sources (Steidel et al. 1996). A redshift for the arc is likely obtainable if it is at $z < 1.3$ since its blue color suggests that it will show strong emission lines in a visual spectrum (Hogg et al. 1998). The arc is unlikely to be at redshift $z > 2.3$ since it shows significant $F300W$ flux.

It is a pleasure to thank Bob Williams and the entire HDF-S team for taking, reducing, and making public the beautiful images of the HDF-S. Scott Burles, Wayne Hu and Inger Joergensen provided very useful help in short order. We thank the referee Emilio Falco for useful comments. This research is based on observations made with the NASA/ESA Hubble Space Telescope, which is operated by AURA under NASA contract NAS 5-26555. Barkana and Blandford acknowledge support by Institute Funds. Hogg acknowledges Hubble Fellowship grant HF-01093.01-97A from

STScI, which is operated by AURA under NASA contract NAS 5-26555.

REFERENCES

- Blandford, R. D., & Narayan, R. 1992, *ARA&A*, 30, 311
- Cohen, J. 1998, personal communication
- Cohen, J. G., Hogg, D. W., Pahre, M. A., Blandford, R., Shopbell, P. L., & Richberg, K., 1998, *ApJS* in press
- Cooray, A. R., Quashnock, J. M., & Miller, M. C. 1998, preprint astro-ph/9806080, to appear in *ApJ*
- Ellis, R. S., *Nature*, 395, A3
- Gwyn, S. 1998, in preparation
- Hogg, D. W., Blandford, R. D., Kundić, T., Fassnacht, C. D., & Malhotra, S. 1996, *ApJ*, 467, L73
- Hogg, D. W., Cohen, J. G., Blandford, R., & Pahre, M. A., 1998, *ApJ* 504 622
- Jorgensen, I., Franx, M., Kjaergaard, P. 1996, *MNRAS*, 280, 167
- Kassiola, A., & Kovner, I. 1993, *ApJ*, 417, 450
- Keeton, C. R., Kochanek, C. S., & Falco, E.E. 1998, *ApJ*, 509, 561
- Kochanek, C. S. 1996, *ApJ*, 466, 638
- Kormann, R., Schneider, P., & Bartelmann, M. 1994, *A&A*, 284, 285
- Madau, P., Pozzetti, L., & Dickinson, M. 1998, *ApJ*, 498, 106
- Pahre, M. A. 1998, *ApJS* submitted
- Ratnatunga, K. U., Ostrander, E. J., Griffiths, R. E. & Im, M. 1995, *ApJ*, 453, L5
- Schneider, P., Ehlers, J., & Falco, E.E. 1992, *Gravitational Lenses* (New York: Springer)
- Steidel, C. C., Giavalisco, M., Dickinson, M. & Adelberger, K. L. 1996, *AJ*, 112, 352
- Turner, E. L., Ostriker, J. P., & Gott, J. R. 1984, *ApJ*, 284, 1
- van Dokkum P. G., Franx M., Kelson D. D., & Illingworth G. D. 1998, *ApJ*, 504, L17
- Williams, R. et al. 1996, *AJ*, 112, 1335
- Williams, R. et al. 1998, in preparation

Williams, R. 1998, personal communication

Zepf, S. E., Moustakas, L. A., & Davis, M. 1997, ApJ, 474, L1

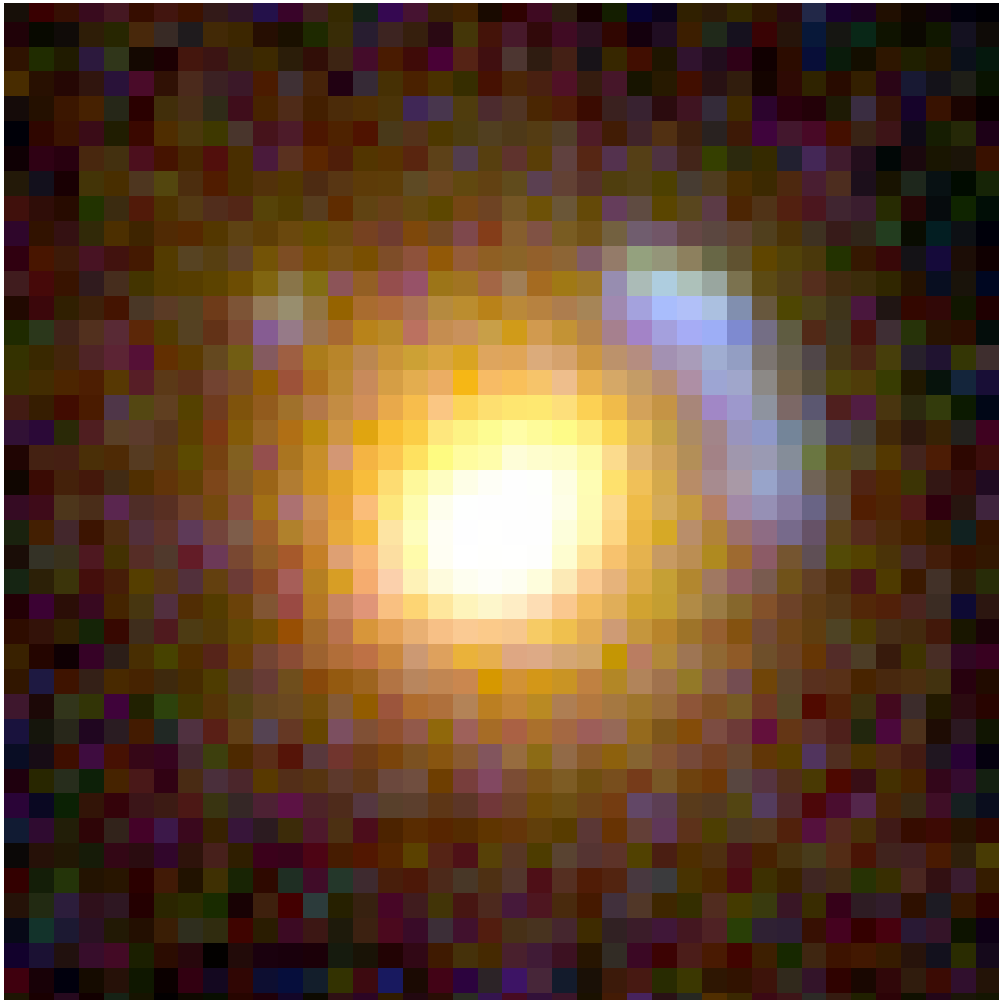


Fig. 1.— A region taken from the public release of the HDF-S (Williams et al. 1998). It shows the lens galaxy, the arc to its NW, and the dot to its NE. North is up and East is to the left (except for a 0.5° rotation). The figure is centered on the lens galaxy and measures $3''.2$ on a side.

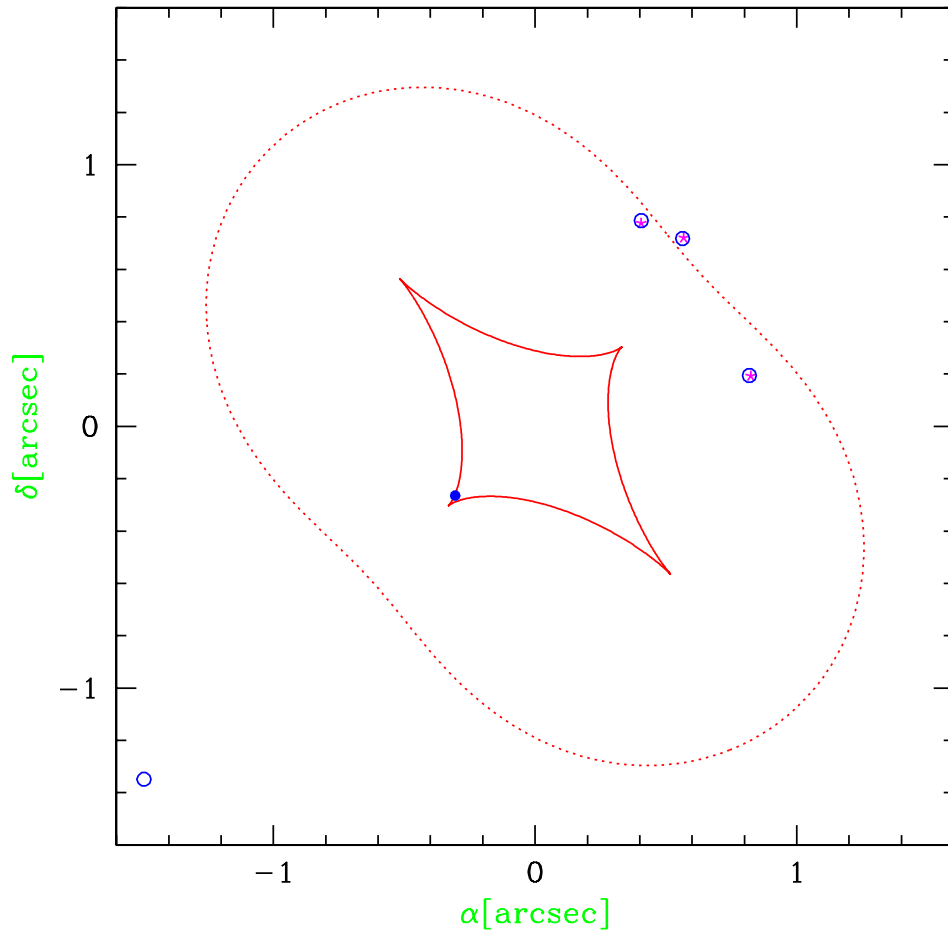


Fig. 2.— Image and source positions for the SIS+ γ [min] model (column 3 of Table 3). Four image positions (\circ) are indicated along with the source position (\bullet) and the observed positions of arc components A , B and D (\star). Also shown are the tangential caustic (solid) and critical curve (dotted). The figure is centered on the lens galaxy, with the α -direction west and the δ -direction north.

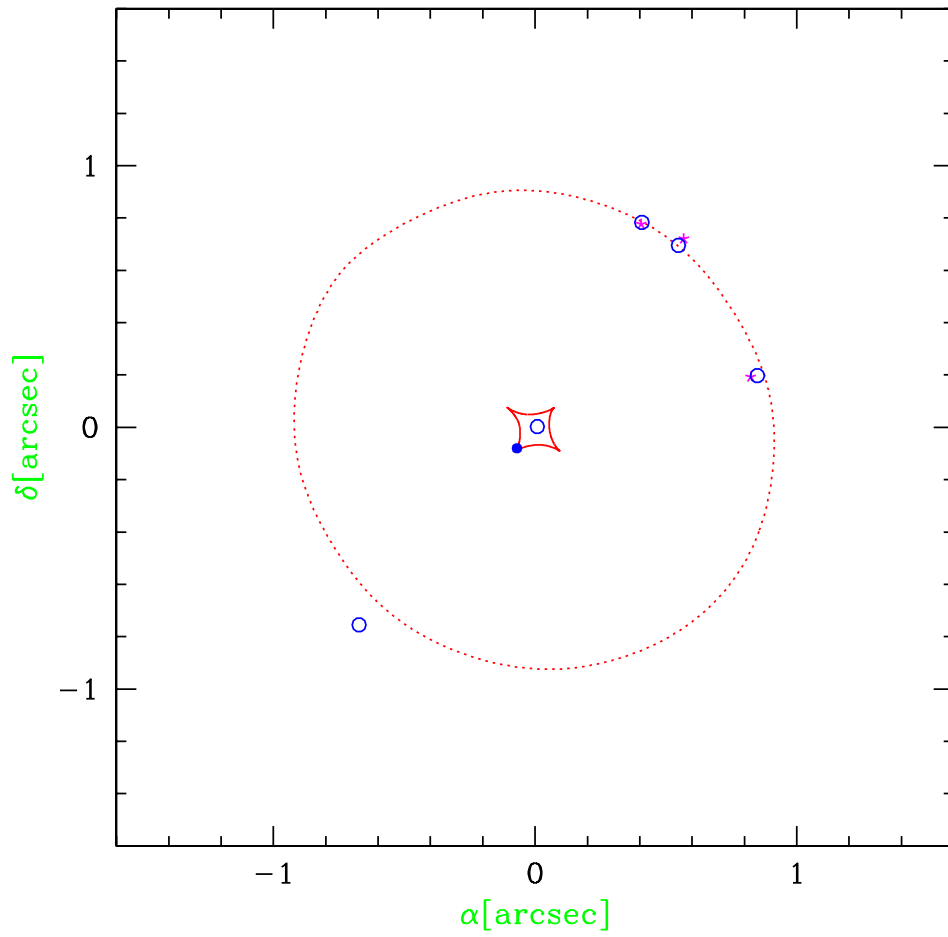


Fig. 3.— Same as Figure 2, but for the M/L+ γ model with $\gamma = 0.05$ (last column of Table 3). There are five images, although the one near the lens center is extremely faint.

Table 1. Photometry

component	flux ^a	[snr] ^b	$F300W - F450W$		$F450W - F606W$		$F606W - F814W$	
	(mag)		(mag)	[snr1,snr2] ^c	(mag)	[snr1,snr2]	(mag)	[snr1,snr2]
elliptical	$F814W = 20.52$	[950]	0.31	[9.2,99]	1.86	[99,610]	1.53	[610,1200]
arc	$F606W = 25.19$	[41]	-0.96	[11,37]	0.24	[37,51]	0.40	[51,37]
dot	$F606W = 28.70$	[6.2]	...	[-1.5,3.9]	0.39	[3.9,6.2]	-0.05	[6.2,2.9]

^aDifferent components have flux measurements in different bands and through different focal-plane apertures; see text for details.

^bSignal-to-noise ratios (snr) measure the flux through the aperture relative to the expected sky noise rms through that same aperture. See text for aperture definitions.

^cThe snr values snr1 and snr2 are for the two bandpasses involved in the color measurement, bluer first.

Table 2. Astrometry^aand Photometry

sub-component	$\Delta\alpha$	$\Delta\delta$	$F450W$ ^b
	(arcsec)	(arcsec)	(mag)
elliptical	0	0	...
arc-A	+0.406	+0.777	27.55
arc-B	+0.568	+0.721	27.43
arc-C	+0.711	+0.478	27.08
arc-D	+0.824	+0.192	28.10
dot	-0.778	+0.567	...

^aPositions are given relative to 22 32 50.9017 -60 32 43.009 (J2000), with the α -direction west and the δ -direction north. We estimate position errors of 0''02 from fitting an artificial image.

^bThe magnitudes of the arc components are based on the fluxes of the fitted gaussians. The fluxes do not add up to the total arc flux because the magnitudes exclude some diffuse emission.

Table 3. Best fit model results

Parameter	SIEMD[min]	SIEMD[maj]	SIS+ γ [min]	SIS+ γ [maj]	M/L	M/L+ γ	M/L+ γ
b or $\bar{\kappa}$	0'85	0'84	1'08	0'87	1.10	1.40	0.998
a or γ	$0.03^{+.97}_{-.03}$	$0.96^{+.04}_{-.74}$	$0.26^{+.04}_{-.05}$	$0.005^{+.18}_{-.005}$...	$0.52^{+.15}_{-.14}$	0.05
θ_ϵ or θ_γ	$41^\circ 2^{+2.9}_{-2.6}$	$-48^\circ 6^{+3.0}_{-3.1}$	$42^\circ 5^{+.7}_{-.7}$	$-49^\circ 0^{+3.5}_{-2.8}$...	$43^\circ 5^{+.5}_{-.5}$	53°.4
#dof	1	1	1	1	3	1	1
$\bar{\chi}^2$	5.1	5.6	0.26	5.8	97	0.40	4.5

Note. — The best fits are formally at $a \rightarrow 0$ for the SIEMD[min] model, at $a \rightarrow 1$ for the SIEMD[maj] model, and at $\gamma \rightarrow 0$ for the SIS+ γ [maj] model. The overall best fit for the M/L+ γ model is given in column 6, while column 7 gives the best fit for this model with the restriction $\gamma = 0.05$. Where given, parameter ranges indicate 1σ uncertainties defined by $\Delta\chi^2 = \bar{\chi}^2$. All angles are measured north through east.